HHS Public Access

Author manuscript

Acta Biomater. Author manuscript; available in PMC 2021 August 01.

Published in final edited form as:

Acta Biomater. 2020 August ; 112: 262–273. doi:10.1016/j.actbio.2020.05.034.

Design and evaluation of collagen-inspired mineral-hydrogel nanocomposites for bone regeneration

Akhil Patel[a], **Samer H. Zaky**[b], **Karen Schoedel**[c], **Hongshuai Li**[d], **Vinayak Sant**[a], **Elia Beniash**[b,e,f], **Charles Sfeir**[b,e,f], **Donna B. Stolz**[c,f,g], **Shilpa Sant**[a,e,f,h]

[a]Department of Pharmaceutical Sciences, School of Pharmacy, University of Pittsburgh, Pittsburgh, PA 15261.

[b]Center for Craniofacial Regeneration, School of Dental Medicine, University of Pittsburgh, Pittsburgh, PA 15261.

[c]Department of Pathology, School of Medicine, University of Pittsburgh, Pittsburgh, PA 15261.

[d]Musculoskeletal Growth & Regeneration Laboratory, Department of Orthopaedic Surgery, School of Medicine, University of Pittsburgh, Pittsburgh, PA 15261.

[e]Department of Bioengineering, Swanson School of Engineering, University of Pittsburgh, Pittsburgh, PA 15219.

[f]McGowan Institute for Regenerative Medicine, Pittsburgh, PA 15260.

[g]Department of Cell Biology, University of Pittsburgh, Pittsburgh, PA 15260.

[h]UPMC Hillman Cancer Center, University of Pittsburgh, Pittsburgh, PA 15260.

Abstract

Bone loss due to trauma and tumors remains a serious clinical concern. Due to limited availability and disease transmission risk with autografts and allografts, calcium phosphate bone fillers and growth factor-based substitute bone grafts are currently used in the clinic. However, substitute grafts lack bone regeneration potential when used without growth factors. When used along with the added growth factors, they lead to unwanted side effects such as uncontrolled bone growth. Collagen-based hydrogel grafts available on the market fail to provide structural guidance to native cells due to high water-solubility and faster degradation. To overcome these limitations, we employed bioinspired material design and fabricated three different hydrogels with structural features similar to native collagen at multiple length-scales. These hydrogels fabricated using

† Corresponding author: Shilpa Sant, PhD, shs149@pitt.edu 3501, 700 Technology Drive, Pittsburgh Technology Center, Pittsburgh PA 15219.

6. Disclosure

Authors declare no conflict of interest.

Declaration of interests

The authors declare that they have no known competing financial interests or personal relationships that could have appeared to influence the work reported in this paper.

polyionic complexation of oppositely charged natural polysaccharides exhibited multi-scale architecture mimicking nanoscale banding pattern, and microscale fibrous structure of native collagen. All three hydrogels promoted biomimetic apatite-like mineral deposition *in vitro* elucidating crystalline structure on the surface while amorphous calcium phosphate inside the hydrogels resulting in mineral-hydrogel nanocomposites. When evaluated in a non-load bearing critical size mouse calvaria defect model, chitosan - kappa carrageenan mineral-hydrogel nanocomposites enhanced bone regeneration without added growth factors compared to empty defect as well as widely used marketed collagen scaffolds. Histological assessment of the regenerated bone revealed improved healing and tissue remodeling with mineral-hydrogel nanocomposites. Overall, these collagen-inspired mineral-hydrogel nanocomposites showed multi-scale hierarchical structure and can potentially serve as promising bioactive hydrogel to promote bone regeneration.

Graphical Abstract

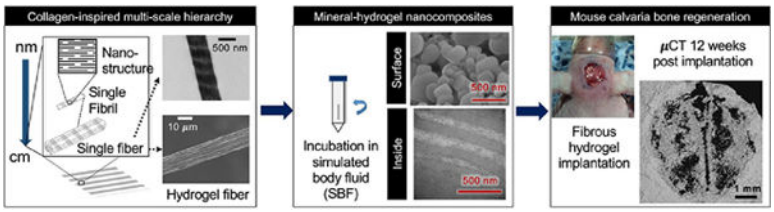

Keywords

Carrageenan; Polysaccharides; Chitosan; Mineral-hydrogel nanocomposites; Calcium phosphate; Bone regeneration; Mouse calvaria defect

1. Introduction

Trauma due to sport injuries, road accidents, and combat lead to loss of bone beyond the capacity of our body to heal. Bone is also lost due to cancer. Synthetic bone grafts made of metal and ceramics are clinically approved but are mostly bio-inert and are employed with the primary purpose of providing mechanical support to the damaged tissue. Additionally, resorbable and non-resorbable metal implants often lead to fibrotic tissue formation around their surface due to delayed bone healing in the area.[1, 2] More recent bone graft substitutes that locally deliver potent growth factors such as bone morphogenic protein-2 (BMP2) exhibit osteoconductive (facilitating new bone growth produced by surrounding mature bone) and osteoinductive (recruitment and differentiation of local progenitor cells, which promote further bone formation) activities. Although use of rhBMP2 makes these bone graft substitutes highly efficacious, BMP2 exhibits several side-effects such as uncontrolled bone growth.[3–5]

Limitations of clinically used bone graft options have led to the development of innovative technologies intended to induce osteogenic bioactivity. Few experimental approaches have aimed to design osteoinductive biomaterials such as silicate nanoparticles [6], bacterial cellulose [7], and biphasic calcium phosphate.[8] At best, osteoinductive bioactivity of these

materials has been attributed to the degradation products of the composite scaffolds.[6, 9] Biomimetic materials can be designed as safer yet functional bioactive alternatives by providing right structural cues to recruit the endogenous cells.[10–13] To mimic natural bone matrix, collagen stands out as the most abundant organic component of the native bone ECM. During the natural bone development, collagen fibrils play arguably the most important role. At molecular scale, collagen is self-assembled from amino acids to form collagen fibrils, which further bundle up as fibers exhibiting multiple length-scale hierarchy. Mineral sequestration, nucleation and growth are considered as three key steps in the process of collagen mineralization.[14–16]. Electrostatic and hydrophobic interactions of collagen, along with its nanoscale arrangement, promotes calcium phosphate sequestration and nucleation while multi-scale structural features of collagen provide an organic template to guide the deposition of inorganic calcium phosphate.[14, 17] Along with the help of other non-collagenous proteins from the ECM, collagen facilitates nucleation of hydroxyapatite (HA) mostly due to its characteristic arrangement of differential electron density and electrostatic charges from the positive net charge close to the C-terminal end of the collagen molecules.[18] In fact, collagen is the most widely used natural biomaterial in the bone graft industry (*e.g.* SpongeCol® from Advanced Biomatrix (San Diego, CA)). Moreover, easy processability of collagen as sponge or gel films provides flexibility making it an attractive commercially available biomaterial. These collagen hydrogels offer advantages to cells through their water-rich microenvironment and sustained delivery of growth factor activity.[19] However, collagen products fail to induce any osteoinductive response when used without osteoinductive biologics such as rhBMP2. Moreover, water-solubility and faster degradation rate of these collagen products make it challenging to provide structural and contact guidance cues to endogenous cells at the implant site over the required time period. Therefore, development of the osteogenic biomaterials as well as innovative fabrication strategies are essential to design an osteogenic biomaterial with multi-scale hierarchy and self-assembly similar to collagen.

Polysaccharides are one such class of polymers with a variety of charge imparting groups such as carboxylate, sulfate, etc.[20], which have been explored to promote mineralization. In fact, electrostatic charges and charge-imparting groups (carboxylate *vs.* sulfate) from polysaccharides have been proven to play important role in biomineralization.[14] Polysaccharides are known to control and guide mineral deposition in marine creatures and crustaceous animals. Chitosan [21, 22] and other polysaccharides such as alginate, [23] gellan gum, [24, 25] etc. either alone or in combination with other polysaccharides have shown to exhibit mineralization potential, which makes them suitable candidates to serve as an organic template for mineral deposition.[26] Due to large chains, most polysaccharides can form bulk hydrogels. However, most of these bulk hydrogel materials lack multi-scale hierarchy as well as strong mechanical properties.

We have recently employed interfacial polyionic complexation (IPC) through the electrostatic interaction at the interface of oppositely charged polysaccharides to fabricate single hydrogel fiber, which exhibited collagen-mimetic dark and light banding pattern at nanoscale.[27] Building on this observation of single hydrogel fiber made of chitosan and gellan gum, we further developed a versatile fabrication platform to collect these individual fibers and align them in parallel to produce fibrous hydrogels (Figure 1A) for multiple

oppositely charged pairs of polysaccharides. These fibers are water insoluble unlike collagen and can readily dry to form thin transparent films and can be rehydrated while maintaining their macroscopic and microscopic structure in various shapes and forms.[28] We employed chitosan (CHT) as the common cationic polysaccharide and tested three different anionic polysaccharides with carboxylate (alginate, ALG and gellan gum, GG) and sulfate (kappa carrageenan, KCA) as functional groups to generate three types of fibrous hydrogels. CHT was chosen as the common positive polyelectrolyte for its proven role in mineralization process in various crustaceous animals such as shrimp.[26] Negatively charged polysaccharides were selected based on their negative charge imparting functional group found in the components of natural ECM. Specifically, alginate (ALG) and gellan gum (GG) contain carboxylate (COO^-) as a negative charge imparting group. Similarly, kappa carrageenan (KCA) was chosen for its sulfate (SO_4^{2-}) group as it is common charge imparting group found in glycosaminoglycan and chondroitin sulfate in natural bone and cartilage ECM.[29]

In this study, we generated hydrogels with fibers aligned parallel to each other and determined their multiscale hierarchical structure, ability to nucleate apatite-like minerals inside and on the surface of the hydrogels *in vitro* and finally, tested ability of non-mineralized hydrogels and mineralized hydrogels (referred throughout as mineral-hydrogel nanocomposites or mineralized hydrogels) to regenerate critical-size mouse calvaria defect. We hypothesized that the collagen-inspired multi-scale hierarchical architecture of mineral-hydrogel nanocomposites along with the electrostatic charges will resemble the features of native bone ECM and promote mineralization and bone regeneration *in vivo.*

2. MATERIALS AND METHODS:

2.1. Materials:

Gellan gum (GG) (G1910), alginic acid (ALG) (A0682), chitosan (CHT) (C3646), and acetic acid (695092) were all purchased from Sigma- Aldrich Co. (St. Louis, MO). The kappa carrageenan (KCA) (C41070) was obtained from Research Products International (Mt. Prospect, IL). Cell culture supplies including Dulbecco's minimum essential medium alpha (DMEM) and Dulbecco's phosphate-buffered saline (DPBS) were purchased from Mediatech Inc. (Manassas, VA) or Corning Inc. (Corning, NY) unless otherwise specified. Fetal bovine serum (FBS) was purchased from Atlanta biologicals Inc. (Flowery Branch, GA).

2.2. Hydrogels fabrication for *in vitro* and *in vivo* studies

Briefly, CHT (1% w/v) solution was prepared in aqueous acetic acid solution (1% w/v). ALG, GG, and KCA (1% w/v) were prepared in distilled water. Two programmable syringe pumps (BS300, Braintree Scientific INC., Braintree, MA) were set at 50mL/h using 10mL syringes connected using a luer-lock three-way valve. The opening of the valve was connected to an 18G needle (REF305185, Becton, Dickinson and Company, Franklin Lakes, NJ). Syringes were jacketed with temperature jackets (BS-SYR-H, Braintree Scientific INC., Braintree, MA) which were set at 60°C. Both the pumps were set at 50mL/h and 14.5mm syringe diameter. To facilitate easy removal of the air-dried fibrous hydrogels, fibers were

manually collected at the tip of the needle using square plastic coverslips (22mm x 22mm, Thermo Fisher Scientific, Waltham, MA) mounted over a glass slide. The plastic cover slips helped detach the dried hydrogels and cut it in precise shapes and dimensions. The fibers were collected in such a way that the fibers were aligned parallel to each other. They were then air-dried and stored until further use. The air-dried hydrogels were cut into 1cm x 0.5cm rectangles and sterilized by submerging them in 70% isopropyl alcohol in DBPS under ultraviolet light in a biosafety cabinet. Hydrogels were then washed three times with sterile DPBS and submerged in sterile DPBS for three hours for hydration followed by incubation in 1X simulated body fluid (SBF, 15mL) at 37°C at 100rpm for 3 or 10 days. SBF was prepared as reported earlier by Kukobo *et al.*[32] Incubation of hydrogels in SBF resulted in the formation of mineral-hydrogel nanocomposites. Non-mineralized hydrogels were used right after DPBS hydration instead of incubation in 1X SBF. Both the mineralized and non-mineralized hydrogels were used for further characterization as described below.

2.3. Scanning Electron Microscopy (SEM)

Following SBF incubation, hydrogels were flash-frozen in liquid nitrogen and lyophilized (Labconco Freezone 4.0, Labconco Corporation, Kansas City, MO). Lyophilized samples were then sputter coated with gold-palladium (5nm thickness) using a Cressington 108 auto sputter coater (Cressington Scientific Instruments, UK). SEM micrographs were obtained using a JEOL 9335 Field Emission SEM (JEOL, Akishima, Japan) at an accelerated voltage of 3kV and a working distance of 8 mm.

2.4. Transmission electron microscopy (TEM)

After 3 days of incubation in SBF, the hydrogels were flash-frozen in liquid nitrogen and were immediately kept for lyophilization as described above. Lyophilized samples were kept in Epon for embedding overnight. The sectioned samples were mounted on carbon grids and were scoped using a JEM-1011 electron microscope (JEOL, Akishima, Japan) at an accelerating voltage of 80kV.

2.5. Fourier transform infrared spectroscopy (FTIR)

Hydrogels or hydrogel-mineral nanocomposites were flash-frozen in liquid nitrogen and lyophilized. The lyophilized materials were crushed along with vacuum dried potassium bromide (KBr) powder using opal mortar and pestle and pressed into a pellet using a hydraulic press. Pure KBr pellets were used to obtain the background spectra. FTIR spectra were acquired in the absorption mode with a resolution of $4cm^{-1}$ using Bruker Vertex 70 FTIR spectrometer (Bruker Corporation, Billerica, MA) with 256 scans collected per spectrum.

2.6. X-ray diffraction spectroscopy

After 3 or 10 days of incubation in SBF, the hydrogels were flash-frozen in liquid nitrogen and were lyophilized overnight. Dried hydrogels were crushed, and the powdered sa ples were tested in Bru er D Discover RD Bru er Corporation, Billerica, Massachusetts) at a generator voltage of 40kV and current of 40mA. The lyophilized hydrogels were crushed using mortar and pestle in order to analyze crystals present in all different orientations. The

2Θ values were exported and plotted using GraphPad Prism 8 (GraphPad Software Inc., San Diego, CA).

2.7. *In vivo* studies: Critical sized mouse calvaria defect and implantation

SKH1 Mice were obtained from Charles River (Wilmington, Massachusetts). Mouse calvaria surgeries were performed according to a protocol (protocol number 13041395) approved by the University of Pittsburgh Institute of Animal Care and Use Committee. Mice were anesthetized using isoflurane (2–5%). The effect of the anesthetic was determined by absent whisker-twitch response and unresponsiveness to gentle, passive extremity extension. Ophthalmic ointment was gently placed on the corneas. The calvaria were prepped with betadine and draped in standard aseptic fashion. The mouse was then numbered using a base three ear notch system. A 1cm sagittal mid-scalp incision was performed, periosteum was retracted, and a 5mm defect was drilled 1 mm anterior to the lambdoid suture in the calvaria bone with a #2 round bur on slow speed handpiece.

Both non-mineralized and mineralized hydrogels were fabricated using filter-sterilized polymer solutions aseptically under a biosafety cabinet and incubated in respective filter-sterilized buffers as described under section 2.2. Prior to use for animal studies, these hydrogels were sterilized one more time by ultraviolet light exposure for one hour in a biosafety cabinet. These hydrogels were either aseptically trimmed into 5mm diameter discs (hydrated mineralized treatment groups) using sterile disposable 5mm biopsy punches (Sklar Surgical Instruments, West Chester, PA) or were flash-frozen and lyophilized prior to trimming into 5mm diameter discs (lyophilized mineralized treatment groups). These hydrogel discs were placed in the defect. The skin wound was closed with resorbable sutures. Eight study groups were evaluated: 1) empty defect control, 2) collagen sponge, 3) CHT-ALG non-mineralized (hydrated), 4) CHT-GG non-mineralized (hydrated), 5) CHT-KCA non-mineralized (hydrated), 6) CHT-KCA mineral-hydrogel nanocomposites (hydrated), 7) CHT-KCA non-mineralized (lyophilized), 8) CHT-KCA mineral-hydrogel nanocomposites (lyophilized). A total of 40 mice (n=5 mice per condition) were employed for the study.

2.8. Micro computed tomography (μCT)

After 12 weeks, the calvaria samples were harvested and fixated by immersion in 4% paraformaldehyde at 4°C and 50rpm for overnight. Following the fixation, the calvaria samples were preserved in 70% ethanol while they were scanned using VivaCT40 (Scanco Medical AG, Bruttisellen, Switzerland) with settings: energy 55 V, intensity 142μA, integration ti e of 300 sec, and isotropic voxel size of 10.5μm. 3D reconstruction of 2D lateral projections was carried out using the operating software interface of VivaCT40.

2.9. Image analysis

FIJI (FIJI is just ImageJ) was used to quantify bone regeneration outcomes based on the 3D reconstructed μCT images. Percentage closure of the defect was determined by first setting the scale using the total defect area of 5mm. Further, wand tool and freehand selection tools were used to annotate the regenerated bone areas to measure the area of regenerated bone. Percentage regenerated bone area of the total defect area was reported and plotted.

2.10. Histological analysis

Histology was performed at the Pitt Biospecimen Core, Health Sciences Core Research Facilities.

Mouse calvaria samples were fixed in 4% paraformaldehyde and subsequently decalcified in an ion-exchange decal unit (BioCare Medical, Pacheco, CA) for 6–8h after μCT imaging. The decalcified calvaria samples were embedded in paraffin and subsequently sectioned along the longitudinal axis using a microtome (Leica Microsystems Inc., Buffalo Grove, IL). The sections were deparaffinized and rehydrated before hematoxylin and eosin (H&E) and Masson's Trichrome staining (HT15, Sigma--Aldrich Co. St. Louis, MO) to assess new bone formation.

2.11. Histomorphometry analysis

H&E and Trichrome stained samples were evaluated using light microscopy by an independent pathologist. A semi-quantitative scoring system was adapted and modified from Vo *et al.* [30] to evaluate healing of the bone defect. Briefly, a score was assigned for a specimen for each study group. A null score (zero) was assigned when the defect site lacked any bone growth or fibrosis activity; H-score of 1 was assigned when the defect site showed presence of histiocytes and new focal immature disorganized bone formation; H-score of 2 was assigned when new bone formation was observed with presence of granulation tissue; H-score of 3 was assigned when incomplete formation of lamellar bone was observed; H-score of 4 was assigned when complete formation of lamellar bone was observed.

2.12. Statistical Analysis

One-way analysis of variance (ANOVA) was employed for statistical analysis using treatment groups as the variable. GraphPad Prism 8 (GraphPad Software Inc., San Diego, CA) was used to conduct the statistical analysis. Statistical significance was determined using adjusted p value fro Tu ey's post-hoc test. P value less than 0.05 was considered as statistically significant. Error bars were indicated based on standard error of mean among five mice of the same treatment group.

3. Results and Discussion

3.1. Fibrous hydrogels exhibit collagen-mimetic multi-scale hierarchy

Positively and negatively charged polysaccharides (1% w/v solutions) were brought in contact with each other at a fixed rate of 50 mL/h in a microfluidic chamber to form fibers at the tip of the needle (Figure 1A) as described earlier.[27, 28] Amine group of CHT interacted with carboxylate group (ALG and GG) or sulfate group (KCA) forming crosslinked interface. Such a crosslinked interface formed continuous fibers when oppositely charged polysaccharides were infused continuously from two syringe pumps. Based on the pairs of the polysaccharides used for the fabrication of fibrous hydrogels, we have abbreviated them as CHT-ALG, CHT-GG, and CHT-KCA. Scanning electron microscopy (SEM) images of single fiber of each type (Figure 1B1, 1C1, and 1D1) revealed multiple fibrils within each fiber whereas transmission electron microscopy (TEM) images of single fiber exhibited periodic regions with differential electron density, which appeared as light

and dark striations at nanoscale for all three polysaccharide pairs (Figure 1B2, C2 and D2). These fibers were collected and arranged manually parallel to each other to produce a bilayer hydrogel with 45 fibers in each layer. Macroscopic structures showed highly swollen fibrous hydrogel structure for all three variants of hydrogels (Figure 1B3, 1C3, and 1D3). Similarly, light microscopy and SEM images of hydrogels exhibited fibrous surface morphology with parallel alignment of fibrils within fibers in the hydrogel (Figure 1B4–5, 1C4–5, and 1D4–D5). Thus, fabricated hydrogel exhibited fibers made up of several fibrils, which appeared to form differential electron density regions at nanoscale through self-assembly similar to collagen fibrils. Collectively, these results suggest that oppositely charged polysaccharides self-assemble to form multi-scale hierarchical fibrous structure. In native collagen, such bottom-up self-assembly of nano-scale building blocks and their hierarchical organization confer unique strength, flexibility and functionality to the tissue at multiple length-scale.[31]

3.2. Fibrous hydrogels promote biomimetic mineral deposition *in vitro*

The ability of biomaterial to promote deposition of calcium phosphate minerals is considered as a predictor of its *in vivo* mineralization bioactivity.[32] In order to simulate *in vitro* mineralization and compare different polysaccharide pairs for their ability to promote mineralization, fibrous hydrogels were incubated in SBF with similar ion concentration to that of human blood plasma.[32] Following three days of incubation in SBF, mineral deposition on the hydrogels was assessed through Alizarin Red S staining (stains for calcium) and its subsequent quantification. CHT-ALG (Supplementary Figure 1A1–A2) showed smaller granular mineral deposits whereas CHT-GG (Supplementary Figure 1B1–B2) and CHT-KCA (Supplementary Figure 1C1–C2) showed relatively larger mineral deposits on the surface of the hydrogels. Moreover, CHT-GG and CHT-KCA exhibited greater extent of mineralization than that of CHT-ALG as confirmed with quantification of alizarin red stain (Supplementary Figure 1D). Further characterization of morphology of minerals deposited on the surface after 3 days of mineralization for CHT-GG (Figure 2A1, 2A2) and CHT-KCA (Figure 2C1, 2C2) showed similar irregular shapes compared to mostly spherical mineral deposits on CHT-ALG (Figure 2B1, 2B2).

A greater extent of mineralization in CHT-GG and CHT-KCA compared to CHT-ALG indicates their better ability to sequester calcium ions from SBF. This stronger affinity to Ca^{2+} is likely due to either polyanionic nature or specific mineral nucleation sites on the surface of CHT-GG and CHT-KCA hydrogel fibers. Tanahashi and Matsuda have reported comparative capacity of functional groups to induce apatite formation in the order of PO_4H_2 > COOH ≫ $CONH_2$ ≃ OH > NH_2 ≫ CH_3 ≃ 0.[33] Although their study did not include sulfate groups, other studies [34, 35] indicated important role of sulfate group for mineralization using sulfated proteoglycans. In case of our mineral-hydrogel nanocomposites, it was observed that both CHT-GG and CHT-KCA showed similar extent of apatite formation on the surface despite their different functional groups (carboxylate and sulfate, respectively) while CHT-ALG and CHT-GG showed significant differences in the extent of apatite formation on the surface. Zeta potential values were comparable in case of GG and KCA. CHT-ALG and CHT-GG possess the same carboxylate functional group; however, average ALG chains had 50% lower zeta potential compared to average GG

chains.[36] This could possibly lead to differences in the available surface charges, thereby facilitating mineral-hydrogel interaction to different extents.

Characterization of three-day mineralized mineral-hydrogel nanocomposites by FTIR showed characteristic peaks of phosphate groups albeit with some differences among the three pairs (Supplementary Figure 1E). For example, typical sharp double peaks observed at approximately around 540 cm^{-1} and 600 cm^{-1}correspond to v_4 vibration of the phosphate group of HA.[37, 38] Indeed, CHT-GG mineral-hydrogel nanocomposites showed a peak at 597.9 cm^{-1} extending as a smooth curve with a tiny shoulder at 617.2 cm^{-1}, whereas CHT-KCA mineral-hydrogel nanocomposites showed peaks at 597.9 cm^{-1} and 626.8 cm^{-1}, although with sharp shoulders. Moreover, the presence of peak at 630 cm^{-1} in both CHT-KCA and CHT-GG mineral-hydrogel nanocomposites further confirms HA-like mineral depositions. On the other hand, CHT-ALG mineral-hydrogel nanocomposites showed a relatively smooth peak at 588.3 cm^{-1}, which resembles a typical smooth peak near 574 cm^{-1} for amorphous calcium phosphate (ACP). Additionally, CHT-ALG, CHT-GG and CHT-KCA mineral-hydrogel nanocomposites showed a sharp peak at 1039 cm^{-1} with a shoulder at 1047, 1053, and 1070 cm^{-1}, respectively, further confirming vibrations of phosphate group (1072–1032 cm^{-1}).[37] Thus, spectra for CHT-GG and CHT-KCA mineral-hydrogel nanocomposites exhibited peaks resembling HA-like apatite whereas peaks in CHT-ALG mineral-hydrogel nanocomposites indicate ACP-like amorphous mineral depositions after three-day mineralization. Taken together, morphological and chemical characterization of mineral-hydrogel nanocomposites indicated that all three pairs provided sites for mineral nucleation within three days of incubation in SBF and promoted growth of biomimetic minerals resulting in mineral-hydrogel nanocomposites.

The differences in mineral morphology observed through SEM of three-day mineralized nanocomposites disappeared in ten-day mineralized nanocomposites (Figure 2A3, B3, and C3) appearing as packed mineral morphology irrespective of the type of nanocomposite. By day 3, the hydrogel surface was still visible (black arrow, Figure 2A1, B1, and C1) while by day 10, almost the entire hydrogel surface was covered with minerals (Figure 2A3, B3, and C3). Thus, the extent of mineralization for each of the three pairs was higher and uniformly distributed after ten-day mineralization compared to their three-day mineralized counterparts.

To further characterize the mineral phase formed by the incubation of hydrogels in SBF, X-ray diffraction (XRD) analysis of mineral-hydrogel nanocomposites was carried out. Crystalline mineral phase was observed in all three types of mineral-hydrogel nanocomposites as shown in Figure 2D1 (three days) and 2D2 (ten days). Interestingly, CHT-KCA mineral-hydrogel nanocomposites (green spectrum) showed more prominent peaks (red arrow) matching with carbonated apatite after both three and ten days of mineralization, whereas CHT-GG and CHT-ALG mineral-hydrogel nanocomposites showed similar carbonated apatite peaks after three days, which was converted to more HA-like peaks after ten days.[39, 40] Such apatite formation on the surface of SBF-incubated biomaterial can be beneficial and can be used as an indicator of bone-bonding (osseointegration) ability when implanted *in vivo*.[32]

Microcomputed tomography (μCT) was performed to confirm uniform distribution of minerals using CHT-GG mineral-hydrogel nanocomposites as an example. Non-mineralized CHT-GG did not show any signal, whereas CHT-GG incubated in SBF for ten days showed uniform distribution of minerals (Figure 2E).

After confirming presence of apatite-like minerals on the surface of mineral-hydrogel nanocomposites as early as 3 days, TEM was employed to evaluate potential of these hydrogels to deposit minerals not only on the surface but also inside the hydrogels. To achieve this, transversely sectioned hydrogel samples were studied using TEM. Relatively lower magnification images (Figure 2F1, 2G1, and 2H1) confirm the presence of minerals inside the hydrogels. Higher magnification images (Figure 2F2, 2G2, 2H2) revealed distinct patterns of mineral deposition for different types of hydrogels. Specifically, CHT-GG and CHT-KCA mineral-hydrogel nanocomposites similarly exhibited smaller size mineral particles (Figure 2B6 and 2C6) while CHT-ALG mineral-hydrogel nanocomposites showed large mineral aggregates in between the fibers (Figure 2A6). These observations can be corroborated by finding from another study. Boskey studied the effect of surface minerals on mineral deposition inside the materials and concluded that mineral deposits on the surface guide crystal orientation within fibrils and also dictate their size and shape.[41]

SEM analysis of CHT-GG and CHT-KCA mineral-hydrogel nanocomposites at three-day time point revealed greater mineral deposition on the surface than on CHT-ALG mineral-hydrogel nanocomposites. Such fast and extensive mineral deposition on the surface could act as a diffusion barrier, preventing infiltration of the calcium phosphate clusters similar to Posner clusters beyond surface in CHT-GG and CHT-KCA and resulting in the smaller size minerals.[42] Posner clusters are considered as a neutral unit of ACP in which central Ca^{2+} ion is surrounded by six phosphate PO_4^{3-} ions, which is further surrounded by eight calcium ions.[42] On the other hand, no significant mineral deposition was observed on the surface of CHT-ALG mineral-hydrogel nanocomposites initially, indicating a slower rate of mineral deposition on the surface of CHT-ALG mineral-hydrogel nanocomposites. This may potentially allow calcium phosphate Posner clusters or saturated mineral liquid phase to easily diffuse inside the hydrogels. As the minerals were sequestered inside the hydrogels to a greater extent in CHT-ALG mineral-hydrogel nanocomposites, they may have started aggregating as seen in Figure 2F1 and 2F2. These data suggest that the diffusion kinetics of mineral ions and/or clusters inside the hydrogels depends on the extent of mineral deposition on the surface. Collectively, the observations of mineral deposits on the surface and inside of the hydrogels are in agreement with widely accepted hypotheses that the amorphous mineral nucleation on surface diffuses inside and transforms into the crystalline phase by losing water over time.[43] We also observed organized mineral deposition along the fiber axes, thus suggesting biomimetic molecular interaction between the minerals and fibers throughout the hydrogel. Altogether, polyionic nature of the polysaccharides in the hydrogels and fibrous alignment may have contributed to the biomimetic mineral-hydrogel nanocomposite formation.

3.3. Lyophilized CHT-KCA mineral-hydrogel nanocomposites promote significant closure of critical-sized calvaria defect after 12-weeks of implantation compared to empty defect

We further evaluated bone regeneration efficacy of these three non-mineralized hydrogels (CHT-GG, CHT-ALG, CHT-KCA) in a critical size (5mm diameter) mouse calvaria defect model. For *in vivo* studies, hydrogels were processed in aseptic conditions and implanted in hydrated form to test their potential for bone regeneration. Surgical implantation of hydrogels in critical size calvaria defect is shown with representative images of exposed calvaria (Figure 3A1), marked defect area (Figure 3A2), and removed calvaria (Figure 3A3). Hydrated hydrogels are often difficult to handle during the surgery and lead to drop-out or misplacement post-implantation [44]; however, our hydrogels were retained in the defect area as seen in Figure 3A4. During the 12-week study period, we did not observe difficulty in movement or sudden weight changes in mice with any of the three types of hydrogels. μCT was employed to quantitate the extent of bone regeneration as well as visualize the spatial distribution of regenerated bone. Out of the three types of hydrogels, CHT-KCA (Supplementary Figure 2A1–A2) exhibited greater bone regeneration than empty defect (control group) after 12 weeks while CHT-GG (Supplementary Figure 2B1–B2) and CHT-ALG (Supplementary Figure 2C1–C2) failed to significantly regenerate bone compared to empty defect control.

Similar to our growth-factor-free approach, Vo *et al.* reported bioactive injectable poly(N-isopropylacrylamide (PNiPAAm) hydrogel implants.[30] PNiPAAm hydrogels mineralized and regenerated rat calvaria defect after 12 weeks without added cells, growth factors or minerals although their early time point of four weeks did not show any bone growth. The mineralization initiation and bone regeneration activity were attributed to hydrophobicity of PNiPAAm hydrogels, whereas we believe that our hydrogels promoted bone regeneration due to its polyionic composition made of polysaccharides with osteogenic potential.

Among the three types of hydrated hydrogels implanted in our study, better performance of CHT-KCA may be attributed to the presence of sulfate group from carrageenan as sulfate has been shown to improve bone regeneration bioactivity.[45–47] Previous studies have demonstrated addition of sulfated polysaccharide along with FDA approved bone void fillers such as JAX™ (β-TCP) to enhance bone regeneration *in vivo* by approximately 20%.[47] This is also in accordance with our observations in *in vitro* mineralization study (Supplementary Figure 4). The difference in three types of hydrogels to facilitate bone growth could also be due to differences in their protein binding ability from serum, which could potentially help attract stem cells and osteoblasts from the surrounding area. Sulfate group in carrageenan has shown to possess greater ability to bind to proteins.[48] In addition, sulfated polysaccharides are known to prevent protein denaturation and prolong its efficacy.[49] Therefore, it is likely that in the case of CHT-KCA, relatively stronger binding of KCA chains to the endogenously produced growth factors at the implant site may have rendered CHT-KCA with higher degree of bone regeneration as compared to CHT-GG and CHT-ALG.

While CHT-KCA showed significantly better bone regeneration than empty defect after 12 weeks, we observed less than 40% closure of the defect (Supplementary Figure 2D). We hypothesized that use of CHT-KCA mineral-hydrogel nanocomposites can further promote

bone regeneration. Indeed, in many studies, calcium phosphate minerals have been utilized for their osteoconductive properties when used as chemically synthesized highly crystalline form such as HA.[50] However, they have been indicated as osteoinductive when HA particles were mixed to form biphasic mixtures with beta tricalcium phosphate (β-TCP) and other amorphous calcium phosphate, with the ability to release calcium and phosphate ions. [51, 52] It should be noted that these are used as a physical mixture and fail to mimic the intricate molecular interactions that occur between inorganic ions and organic matrix at multiple length scale during formation of natural nanocomposite like bone. Our hydrogels might have enabled the formation of organic-inorganic nanocomposites containing crystalline apatite with carbonated substitutions. These nanocomposites appeared as biphasic mixture rendering advantages of both the crystalline apatite and amorphous calcium phosphate. Therefore, to further increase the bone regeneration bioactivity of CHT-KCA, CHT-KCA mineral-hydrogel nanocomposites were implanted in the critical size (5mm) mouse calvaria defect. CHT-KCA mineral-hydrogel nanocomposites were aseptically fabricated using sterile SBF and implanted in mice in hydrated form. Indeed, the extent of closure with CHT-KCA mineral-hydrogel nanocomposites (Figure 3D1–3D2) was significantly improved compared to the empty defect (Figure 3B1–3B2). However, mineral-hydrogel nanocomposites enhanced the defect closure only by 5–10% compared to CHT-KCA hydrogels (non-mineralized) (Figure 3E1). This marginal improvement in defect closure was attributed to wash-out of some mineral deposits due to excessive saline washing at the defect site following bleeding, since the CHT-KCA mineral-hydrogel nanocomposites were implanted in hydrated form directly after their removal from sterile SBF.

In order to preserve deposited minerals on mineral-hydrogel nanocomposites, the CHT-KCA mineral-hydrogel nanocomposites was processed in lyophilized form after 10 days of incubation in SBF prior to its implantation.[32] Lyophilization of biomaterials preserves the architecture, [53] makes it less prone to bacterial infection and improves its shelf-life. Preservation of mineral deposits while maintaining porosity of the mineral-hydrogel nanocomposites is essential to ensure its bioactivity. Indeed, lyophilized CHT-KCA mineral-hydrogel nanocomposites showed greater bone regeneration (Figure 3D3–3D4, 53±18% defect closure**)** compared to its non-mineralized counterpart (Figure 3C3–3C4, 30±10% defect closure), lyophilized collagen sponge used as a positive control (Figure 3B3–3B4, 26±13% defect closure) and empty defect group (Figure 3B3–B4, 7±4% defect closure). Thus, lyophilized CHT-KCA mineral-hydrogel nanocomposites showed significantly higher closure compared to both empty defect group and lyophilized collagen sponge (Figure 3E). However, lyophilized form was not significantly different compared to the hydrated form due to large biological variation among five mice. Similarly, both non-mineralized hydrogels and mineral-hydrogel nanocomposites in the lyophilized form did not show statistically significant differences in the defect closure (only about 13%). This could be attributed to the synergistic effect of the sulfate group of KCA and presence of both crystalline and amorphous calcium phosphate minerals. In fact, similar study by Rai *et al.* employed combination of β-TCP and heparin sulfate, which enhanced bone regeneration by 20% in rabbit ulna defect compared to β-TCP alone treatment group.[47] Since their study did not include heparin sulfate alone condition as a non-mineralized control, it is not possible to comment on the exact role of sulfated polysaccharides for enhanced bone regeneration.

In a similar approach, Shao *et al.* determined efficacy of nanohydroxyapatite (nHA) with or without BMP2 peptide covalently immobilized in an *in situ* forming GelMA hydrogel.[54] Their GelMA-nHA group (without BMP2) did not show significant bone regeneration compared to control after 4 or 12 weeks of implantation in 5mm rat calvaria defect whereas our hydrogels enhanced bone regeneration without any added growth factors, which can be attributed to the influence of organized anisotropic assembly of mineral-fiber composites. Additionally, the surface crystalline deposits could have led to the protein adsorption due to nano-/submicron-scale surface roughness and surface electrostatic charges.[55, 56] Moreover, amorphous mineral deposits inside the hydrogels and resorption of crystalline minerals may have created a calcium and phosphate rich microenvironment similar to inorganic mixture of biphasic calcium phosphate consisting of HA and β-TCP.[52, 57, 58] In separate studies, calcium ions from such microenvironments have been shown to stimulate mature bone cells via nitric oxide formation and to stimulate osteoblasts through extracellular signal–regulated kinases 1/2 (ERK 1/2) pathway [59, 60]. On the other hand, phosphate ions, which exists mostly in PO_4^{3-} form have been shown to regulate growth and differentiation of osteoblasts via ERK1/2 and insulin-like growth factor 1 (IGF-1) pathways and are also known to increase the BMP expression.[61–63] Collectively, the presence of both crystalline and amorphous mineral deposits on the surface and inside the mineral-hydrogel nanocomposites together with bioinspired multi-scale fibrous architecture of hydrogels may have conferred bone regeneration bioactivity to mineral-hydrogel nanocomposites.

3.4. Histological evaluation of the regenerated mouse calvaria showed better healing mouse with hydrogel implants compared to empty defect

We performed histology on the regenerated defect area to evaluate the quality of the regenerated bone among the different treatment groups (empty defect, lyophilized non-mineralized CHT-KCA hydrogels, and lyophilized CHT-KCA mineral-hydrogel nanocomposites). Two regions of interest were identified as 1) new bone region (NB) (color-coded as green box) and 2) native old bone (OB) (color-coded as purple box). Empty defect group (control, Figure 4A1, 4A2, 4A3) showed limited bone growth. Further detailed evaluation of the NB region (green) showed absence of bone cells and demonstrated mainly brain tissue underneath the defect (Figure 4A4–4A5). The NB region of the empty defect contained hemosiderin-laden macrophages (Figure 4A6–4A7), representing cellular response to the defect. Based on the overall morphology and organization of regenerated bone, the healing score (H-Score) of the NB region reflected a null score out of four (Table 2). The treatment group with CHT-KCA hydrogels (Figure 4B1, 4B2, 4B3) showed focal hemosiderin, focal immature and disorganized bone as well as presence of histiocytes and lymphocytes indicating focal bone regeneration activity in the NB region (Figure 4B4–4B5), whereas a lining of immature bone at the defect edge was seen near the OB region (Figure 4B6–4B7). Immature and disorganized bone in the NB region reflected an H-score of one out of four (Table 2). Interestingly, the CHT-KCA mineral-hydrogel nanocomposites (Figure 4C1, 4C2, 4C3) group revealed granulation tissue, presence of immature bone, histiocytes, and neutrophils indicating greater extent of focal bone growth in the NB region (Figure 4C4–4C5) compared to non-mineralized CHT-KCA. The presence of granulation tissue in the NB region was reflected by an H-score of two out of four (Table 2). Additionally, the

collagen organization of bone in the NB region was highest in the CHT-KCA mineral-hydrogel nanocomposites group among the three treatment conditions. We found two studies where growth factor-free materials were tested in calvaria defects of rabbit and rat.[7, 30] Specifically, Koike *et al.* observed immature bone around bacterial cellulose matrix populated with osteoblasts in a rabbit frontal sinus model.[7] They also found that the bacterial cellulose matrix improved the quality of regenerated bone more than the BMP2 alone group due to superior recruitment and 3D organization of the incoming host cells. Additionally, the inflammatory response to our hydrogels was less than that of the hydrogels implanted by Vo *et al.* in the rat calvaria defect, which follows similar bone regeneration physiology and steps as compared to that of mouse calvaria defect.[30] In contrast to their observation, we did not observe any prominent features of fibrotic capsule formation, although the presence of fibrosis and histiocytes could point to inflammatory response essential for bone repair.

Bone regeneration in the calvaria region is believed to occur via an intramembranous mechanism whereby mesenchymal cells differentiate into osteoblasts, deposit osteoid, which, in turn, calcify to become woven bone.[64] Through histologic study of CHT-KCA mineral-hydrogel nanocomposites, we observed that regenerated bone was a result of both the intramembranous bone regeneration (Supplementary Figure 3A1–3A2) and endochondral ossification (Supplementary Figure 3B1) although intramembranous growth was dominant. This suggested partial contribution of chondrogenesis-mediated bone growth in otherwise intramembranous bone growth. Indeed, some studies [65, 66] have successfully demonstrated implantation of *in vitro* chondrogenesis primed cells to enhance bone regeneration in skull defects.

Collectively, the mineral-hydrogel nanocomposites demonstrated collagen-inspired structural features at multiple length-scale, which enhanced bone regeneration in a critical size mouse calvaria defect model without the use of added growth factors. We acknowledge that we did not observe complete defect closure using the mineral-hydrogel nanocomposite alone, which may imply our material may perform better when supplemented with growth factors. However, given the ability of mineral-hydrogel nanocomposite to enhance bone regeneration on its own, we envision that we may need reduced dose of growth factors to achieve complete defect closure. These results suggest that bioinspired bone grafts with multiscale hierarchy have potential to serve as functional templates to design better osteogenic biomaterials.

4. Conclusions

Interfacial mixing of oppositely charged polysaccharides resulted in collagen-inspired multi-scale hierarchical structure. Incubation of these fibrous hydrogels in SBF led to deposition of biomimetic minerals as early as three days. Additionally, the mineral-hydrogel nanocomposites showed apatite-like minerals on the surface and amorphous calcium phosphate minerals within the hydrogels. When compared, the CHT-KCA hydrogels showed the most promising bioactivity to enhance bone regeneration in a critical-sized mouse calvaria defect without use of added growth factors. Moreover, lyophilized form of CHT-KCA mineral-hydrogel nanocomposites was more efficacious in regenerating mouse calvaria

than empty defect control as well as collagen sponge, and resulted in better healing of the tissue. Based on these results, our collagen-inspired mineral-hydrogel nanocomposites have potential to enhance bone regeneration and can potentially be used as carrier scaffolds to reduce the currently used dose of growth factors for bone regeneration.

Supplementary Material

Refer to Web version on PubMed Central for supplementary material.

Acknowledgements

This project was supported by the start-up funds from University of Pittsburgh School of Pharmacy, partly supported by award number P30CA047904 from the National Cancer Institute, and with support from the Henry L. Hillman Foundation, and pilot funding from Center for Medical Innovation, Swanson School of Engineering, University of Pittsburgh to SS; and Graduate Research Fellowship award from the University of Pittsburgh School of Pharmacy to AP. This project used the UPMC Hillman Cancer Center and Tissue and Research Pathology/Pitt Biospecimen Core shared resource for histology, which is supported in part by award P30CA047904. Authors also thank Anthony Green and Paul Knizner for their service for histology. Authors thank Kelly Hoffman at the Division of Laboratory Animals and Resources at University of Pittsburgh for her help with mice housing. Authors acknowledge Dr. Abhijit Roy for help with microCT data export. This work (specifically, XRD) was performed at the Nanoscale Fabrication and Characterization Facility, a laboratory of the Gertrude E. and John M. Petersen Institute of NanoScience and Engineering, housed at the University of Pittsburgh.

7. References:

[1]. Amini AR, Wallace JS, Nukavarapu SP, Short-term and long-term effects of orthopedic biodegradable implants, J Long Term Eff Med Implants 21(2) (2011) 93–122. [PubMed: 22043969]

[2]. Vale FM, Castro M, Monteiro J, Couto FS, Pinto R, Giao Toscano Rico JM, Acrylic bone cement induces the production of free radicals by cultured human fibroblasts, Biomaterials 18(16) (1997) 1133–5. [PubMed: 9247352]

[3]. David SM, Gruber HE, Meyer RA Jr., Murakami T, Tabor OB, Howard BA, Wozney JM, Hanley EN Jr., Lumbar spinal fusion using recombinant human bone morphogenetic protein in the canine A comparison of three dosages and two carriers, Spine (Phila Pa 1976) 24(19) (1999) 1973–9. [PubMed: 10528370]

[4]. Terrell TG, Working PK, Chow CP, Green JD, Pathology of recombinant human transforming growth factor-beta 1 in rats and rabbits, Int Rev Exp Pathol 34 Pt B (1993) 43–67. [PubMed: 8458717]

[5]. Fujimoto R, Tanizawa T, Nishida S, Yamamoto N, Soshi S, Endo N, Takahashi HE, Local effects of transforming growth factor-beta1 on rat calvaria: changes depending on the dose and the injection site, J Bone Miner Metab 17(1) (1999) 11–7. [PubMed: 10084396]

[6]. Gaharwar AK, Mihaila SM, Swami A, Patel A, Sant S, Reis RL, Marques AP, Gomes ME, Khademhosseini A, Bioactive Silicate Nanoplatelets for Osteogenic Differentiation of Human Mesenchymal Stem Cells, Advanced Materials 25(24) (2013) 3329–3336. [PubMed: 23670944]

[7]. Koike T, Sha JJ, Bai YP, Matsuda Y, Hideshima K, Yamada T, Kanno T, Efficacy of Bacterial Cellulose as a Carrier of BMP-2 for Bone Regeneration in a Rabbit Frontal Sinus Model, Materials 12(15) (2019).

[8]. Lobo SE, Arinzeh TL, Biphasic Calcium Phosphate Ceramics for Bone Regeneration and Tissue Engineering Applications, Materials 3(2) (2010) 815–826.

[9]. Xavier JR, Thakur T, Desai P, Jaiswal MK, Sears N, Cosgriff-Hernandez E, Kaunas R, Gaharwar AK, Bioactive nanoengineered hydrogels for bone tissue engineering: a growth-factor-free approach, ACS Nano 9(3) (2015) 3109–18. [PubMed: 25674809]

[10]. Patel A, Mukundan S, Wang W, Karumuri A, Sant V, Mukhopadhyay SM, Sant S, Carbon-based hierarchical scaffolds for myoblast differentiation: Synergy between nano-functionalization and alignment, Acta Biomater 32 (2016) 77–88. [PubMed: 26768231]

[11]. Patel A, Xue Y, Mukundan S, Rohan LC, Sant V, Stolz DB, Sant S, Cell-Instructive Graphene-Containing Nanocomposites Induce Multinucleated Myotube Formation, Ann Biomed Eng 44(6) (2016) 2036–48. [PubMed: 26983841]

[12]. Sant S, Coutinho DF, Sadr N, Reis RL, Khademhosseini A, Tissue Analogs by the Assembly of Engineered Hydrogel Blocks, Biomimetic Approaches for Biomaterials Development, Wiley-VCH Verlag GmbH & Co 2012, pp. 471–493.

[13]. Sant S, Hancock MJ, Donnelly JP, Iyer D, Khademhosseini A, Biomimetic gradient hydrogels for tissue engineering, Can J Chem Eng 88(6) (2010) 899–911. [PubMed: 21874065]

[14]. Landis WJ, An overview of vertebrate mineralization with emphasis on collagen-mineral interaction, Gravit Space Biol Bull 12(2) (1999) 15–26. [PubMed: 11541779]

[15]. Ottani V, Raspanti M, Ruggeri A, Collagen structure and functional implications, Micron 32(3) (2001) 251–260. [PubMed: 11006505]

[16]. Tzaphlidou M, The role of collagen in bone structure: An image processing approach, Micron 36(7–8) (2005) 593–601. [PubMed: 16209926]

[17]. Olszta MJ, Cheng X, Jee SS, Kumar R, Kim Y-Y, Kaufman MJ, Douglas EP, Gower LB, Bone structure and formation: A new perspective, Materials Science and Engineering: R: Reports 58(3–5) (2007) 77–116.

[18]. Nudelman F, Pieterse K, George A, Bomans PH, Friedrich H, Brylka LJ, Hilbers PA, de With G, Sommerdijk NA, The role of collagen in bone apatite formation in the presence of hydroxyapatite nucleation inhibitors, Nat Mater 9(12) (2010) 1004–9. [PubMed: 20972429]

[19]. Shekaran A, Garcia JR, Clark AY, Kavanaugh TE, Lin AS, Guldberg RE, Garcia AJ, Bone regeneration using an alpha 2 beta 1 integrin-specific hydrogel as a BMP-2 delivery vehicle, Biomaterials 35(21) (2014) 5453–5461. [PubMed: 24726536]

[20]. Yamanlar S, Sant S, Boudou T, Picart C, Khademhosseini A, Surface functionalization of hyaluronic acid hydrogels by polyelectrolyte multilayer films, Biomaterials 32(24) (2011) 5590–9. [PubMed: 21571364]

[21]. Madihally SV, Matthew HWT, Porous chitosan scaffolds for tissue engineering, Biomaterials 20(12) (1999) 1133–1142. [PubMed: 10382829]

[22]. Di Martino A, Sittinger M, Risbud MV, Chitosan: A versatile biopolymer for orthopaedic tissue-engineering, Biomaterials 26(30) (2005) 5983–5990. [PubMed: 15894370]

[23]. Rubert M, Monjo M, Lyngstadaas SP, Ramis JM, Effect of alginate hydrogel containing polyproline-rich peptides on osteoblast differentiation, Biomedical Materials 7(5) (2012) 055003.

[24]. Stevens LR, Gilmore KJ, Wallace GG, in het Panhuis M, Tissue engineering with gellan gum, Biomaterials Science 4(9) (2016) 1276–1290. [PubMed: 27426524]

[25]. Douglas TEL, Piwowarczyk W, Pamula E, Liskova J, Schaubroeck D, Leeuwenburgh SCG, Brackman G, Balcaen L, Detsch R, Declercq H, Cholewa-Kowalska K, Dokupil A, Cuijpers VMJI, Vanhaecke F, Cornelissen R, Coenye T, Boccaccini AR, Dubruel P, Injectable self-gelling composites for bone tissue engineering based on gellan gum hydrogel enriched with different bioglasses, Biomed Mater 9(4) (2014) 045014.

[26]. Giuffre AJ, Hamm LM, Han N, De Yoreo JJ, Dove PM, Polysaccharide chemistry regulates kinetics of calcite nucleation through competition of interfacial energies, Proc Natl Acad Sci U S A 110(23) (2013) 9261–6. [PubMed: 23690577]

[27]. Sant S, Coutinho DF, Gaharwar AK, Neves NM, Reis RL, Gomes ME, Khademhosseini A, Self-Assembled Hydrogel Fiber Bundles from Oppositely Charged Polyelectrolytes Mimic Micro-/Nanoscale Hierarchy of Collagen, Advanced Functional Materials 27(36) (2017) 1606273 (1–10).

[28]. Patel A, Xue Y, Hartley R, Sant V, Eles JR, Cui XT, Stolz DB, Sant S, Hierarchically aligned fibrous hydrogel films through microfluidic self-assembly of graphene and polysaccharides, Biotechnology and Bioengineering 115(10) (2018) 2654–2667. [PubMed: 30011077]

[29]. Yang B, Bhattacharyya S, Linhardt R, Tobacman J, Exposure to common food additive carrageenan leads to reduced sulfatase activity and increase in sulfated glycosaminoglycans in human epithelial cells, Biochimie 94(6) (2012) 1309–16. [PubMed: 22410212]

[30]. Vo TN, Ekenseair AK, Spicer PP, Watson BM, Tzouanas SN, Roh TT, Mikos AG, In vitro and in vivo evaluation of self-mineralization and biocompatibility of injectable, dual-gelling hydrogels

for bone tissue engineering, Journal of Controlled Release 205 (2015) 25–34. [PubMed: 25483428]

[31]. Beniash E, Biominerals—hierarchical nanocomposites: the example of bone, Wiley Interdisciplinary Reviews: Nanomedicine and Nanobiotechnology 3(1) (2011) 47–69. [PubMed: 20827739]

[32]. Kokubo T, Takadama H, How useful is SBF in predicting in vivo bone bioactivity?, Biomaterials 27(15) (2006) 2907–15. [PubMed: 16448693]

[33]. Tanahashi M, Matsuda T, Surface functional group dependence on apatite formation on self-assembled monolayers in a simulated body fluid, Journal of Biomedical Materials Research 34(3) (1997) 305–315. [PubMed: 9086400]

[34]. Arias JL, Neira-Carrillo A, Arias JI, Escobar C, Bodero M, David M, Fernández MS, Sulfated polymers in biological mineralization: a plausible source for bio-inspired engineering, Journal of Materials Chemistry 14(14) (2004) 2154–2160.

[35]. Carrino DA, Rodriguez JP, Caplan AI, Dermatan sulfate proteoglycans from the mineralized matrix of the avian eggshell, Connective Tissue Research 36(3) (1997) 175–193. [PubMed: 9512887]

[36]. Patel A, Sant V, Velankar S, Dutta M, Balasubramanyam V, Sane P, Agrawal V, Wilson J; Rohan L, Sant S, Self-assembly of multi-scale anisotropic hydrogels through interfacial polyionic complexation, In Press (2020).

[37]. Koutsopoulos S, Synthesis and characterization of hydroxyapatite crystals: a review study on the analytical methods, J Biomed Mater Res 62(4) (2002) 600–12. [PubMed: 12221709]

[38]. Zhang X, Li Y, Sun X, Kishen A, Deng X, Yang X, Wang H, Cong C, Wang Y, Wu M, Biomimetic remineralization of demineralized enamel with nano-complexes of phosphorylated chitosan and amorphous calcium phosphate, J Mater Sci Mater Med (2014).

[39]. Pishbin F, Mouriño V, Flor S, Kreppel S, Salih V, Ryan MP, Boccaccini AR, Electrophoretic deposition of gentamicin-loaded bioactive glass/chitosan composite coatings for orthopaedic implants, ACS Appl Mater Interfaces 6(11) (2014) 8796–806. [PubMed: 24827466]

[40]. Lala S, Brahmachari S, Das PK, Das D, Kar T, Pradhan SK, Biocompatible nanocrystalline natural bonelike carbonated hydroxyapatite synthesized by mechanical alloying in a record minimum time, Mater Sci Eng C Mater Biol Appl 42 (2014) 647–56. [PubMed: 25063165]

[41]. Boskey AL, Mineral analysis provides insights into the mechanism of biomineralization, Calcif Tissue Int 72(5) (2003) 533–6. [PubMed: 12704568]

[42]. Posner AS, Betts F, Synthetic amorphous calcium phosphate and its relation to bone mineral structure, Accounts of Chemical Research 8(8) (1975) 273–281.

[43]. Chen L, Jacquet R, Lowder E, Landis WJ, Refinement of collagen-mineral interaction: A possible role for osteocalcin in apatite crystal nucleation, growth and development, Bone (2014).

[44]. Yamada N, Kim WC, Yoshida T, Oka Y, Ikeda T, Fujiwara H, Nishida A, Matsuda KI, Tabata Y, Kawata M, Kubo T, Effect of Gelatin beta-tricalcium Phosphate Sponge with Platelet-rich Plasma on Bone Regeneration in Massive Ulna Defects, Journal of Medical and Biological Engineering 33(6) (2013) 545–551.

[45]. Takada T, Katagiri T, Ifuku M, Morimura N, Kobayashi M, Hasegawa K, Ogamo A, Kamijo R, Sulfated polysaccharides enhance the biological activities of bone morphogenetic proteins, Journal of Biological Chemistry 278(44) (2003) 43229–43235. [PubMed: 12912996]

[46]. Zhou HJ, Qian JC, Wang J, Yao WT, Liu CS, Chen JG, Cao XH, Enhanced bioactivity of bone morphogenetic protein-2 with low dose of 2-N, 6-O-sulfated chitosan in vitro and in vivo, Biomaterials 30(9) (2009) 1715–1724. [PubMed: 19131102]

[47]. Rai B, Chatterjea A, Lim ZXH, Tan TC, Sawyer AA, Hosaka YZ, Murali S, Lee JJL, Fenwick SA, Hui JH, Nurcombe V, Cool SM, Repair of segmental ulna defects using a beta-TCP implant in combination with a heparan sulfate glycosaminoglycan variant, Acta Biomaterialia 28 (2015) 193–204. [PubMed: 26384700]

[48]. Baeza RI, Carp DJ, Perez OE, Pilosof AMR, kappa-carrageenan - Protein interactions: Effect of proteins on polysaccharide gelling and textural properties, Lebensmittel-Wissenschaft Und-Technologie-Food Science and Technology 35(8) (2002) 741–747.

[49]. Sun CY, Liu MX, Sun PW, Yang MM, Yates EA, Guo ZK, Fernig DG, Sulfated polysaccharides interact with fibroblast growth factors and protect from denaturation, Febs Open Bio 9(8) (2019) 1477–1487.

[50]. Jeong J, Kim JH, Shim JH, Hwang NS, Heo CY, Bioactive calcium phosphate materials and applications in bone regeneration, Biomater Res 23 (2019) 4. [PubMed: 30675377]

[51]. Ogata K, Imazato S, Ehara A, Ebisu S, Kinomoto Y, Nakano T, Umakoshi Y, Comparison of osteoblast responses to hydroxyapatite and hydroxyapatite/soluble calcium phosphate composites, J Biomed Mater Res A 72(2) (2005) 127–35. [PubMed: 15625683]

[52]. Ramay HR, Zhang M, Biphasic calcium phosphate nanocomposite porous scaffolds for load-bearing bone tissue engineering, Biomaterials 25(21) (2004) 5171–80. [PubMed: 15109841]

[53]. Xia H, Zhao D, Zhu H, Hua Y, Xiao K, Xu Y, Liu Y, Chen W, Liu Y, Zhang W, Liu W, Tang S, Cao Y, Wang X, Chen HH, Zhou G, Lyophilized Scaffolds Fabricated from 3D-Printed Photocurable Natural Hydrogel for Cartilage Regeneration, ACS Appl Mater Interfaces 10(37) (2018) 31704–31715. [PubMed: 30157627]

[54]. Shao N, Guo J, Guan Y, Zhang H, Li X, Chen X, Zhou D, Huang Y, Development of Organic/Inorganic Compatible and Sustainably Bioactive Composites for Effective Bone Regeneration, Biomacromolecules 19(9) (2018) 3637–3648. [PubMed: 30049206]

[55]. dos Santos EA, Farina M, Soares GA, Anselme K, Surface energy of hydroxyapatite and beta-tricalcium phosphate ceramics driving serum protein adsorption and osteoblast adhesion, J Mater Sci Mater Med 19(6) (2008) 2307–16. [PubMed: 18157507]

[56]. Tsapikouni TS, Allen S, Missirlis YF, Measurement of interaction forces between fibrinogen coated probes and mica surface with the atomic force microscope: The pH and ionic strength effect, Biointerphases 3(1) (2008) 1–8. [PubMed: 20408656]

[57]. Liu F, Liu Y, Li X, Wang X, Li D, Chung S, Chen C, Lee IS, Osteogenesis of 3D printed macro-pore size biphasic calcium phosphate scaffold in rabbit calvaria, J Biomater Appl 33(9) (2019) 1168–1177. [PubMed: 30665312]

[58]. Amirian J, Linh NT, Min YK, Lee BT, Bone formation of a porous Gelatin-Pectin-biphasic calcium phosphate composite in presence of BMP-2 and VEGF, Int J Biol Macromol 76 (2015) 10–24. [PubMed: 25709009]

[59]. Riddle RC, Taylor AF, Genetos DC, Donahue HJ, MAP kinase and calcium signaling mediate fluid flow-induced human mesenchymal stem cell proliferation, Am J Physiol Cell Physiol 290(3) (2006) C776–84. [PubMed: 16267109]

[60]. Foreman MA, Gu Y, Howl JD, Jones S, Publicover SJ, Group III metabotropic glutamate receptor activation inhibits Ca2+ influx and nitric oxide synthase activity in bone marrow stromal cells, J Cell Physiol 204(2) (2005) 704–13. [PubMed: 15799084]

[61]. Tada H, Nemoto E, Foster BL, Somerman MJ, Shimauchi H, Phosphate increases bone morphogenetic protein-2 expression through cAMP-dependent protein kinase and ERK1/2 pathways in human dental pulp cells, Bone 48(6) (2011) 1409–16. [PubMed: 21419244]

[62]. Julien M, Khoshniat S, Lacreusette A, Gatius M, Bozec A, Wagner EF, Wittrant Y, Masson M, Weiss P, Beck L, Magne D, Guicheux J, Phosphate-dependent regulation of MGP in osteoblasts: role of ERK1/2 and Fra-1, J Bone Miner Res 24(11) (2009) 1856–68. [PubMed: 19419315]

[63]. Khoshniat S, Bourgine A, Julien M, Weiss P, Guicheux J, Beck L, The emergence of phosphate as a specific signaling molecule in bone and other cell types in mammals, Cell Mol Life Sci 68(2) (2011) 205–18. [PubMed: 20848155]

[64]. Bullough PG, Orthopaedic pathology, Expert consult Online and print, Mosby/Elsevier, Philadelphia, PA, 2009.

[65]. Montufar-Solis D, Nguyen HC, Nguyen HD, Horn WN, Cody DD, Duke PJ, Using cartilage to repair bone: an alternative approach in tissue engineering, Ann Biomed Eng 32(3) (2004) 504–9. [PubMed: 15095824]

[66]. Dennis SC, Berkland CJ, Bonewald LF, Detamore MS, Endochondral ossification for enhancing bone regeneration: converging native extracellular matrix biomaterials and developmental engineering in vivo, Tissue Eng Part B Rev 21(3) (2015) 247–66. [PubMed: 25336144]

Statement of Significance

Hydrogels, especially collagen, are widely used in bone tissue engineering. Collagen fibrils play arguably the most important role during natural bone development. Its multi-scale hierarchical structure to form fibers from fibrils and electrostatic charges enable mineral sequestration, nucleation, and growth. However, bulk collagen hydrogels exhibit limited bone regeneration and are mostly used as carriers for highly potent growth factors such as bone morphogenic protein-2, which increase the risk of uncontrolled bone growth. Thus, there is an unmet clinical need for a collagen-inspired biomaterial that can recreate structural hierarchy, mineral sequestration ability, and stimulate recruitment of host progenitor cells to facilitate bone regeneration. Here, we propose collagen-inspired bioactive mineral-hydrogel nanocomposites as a growth factor-free approach to guide and enhance bone regeneration.

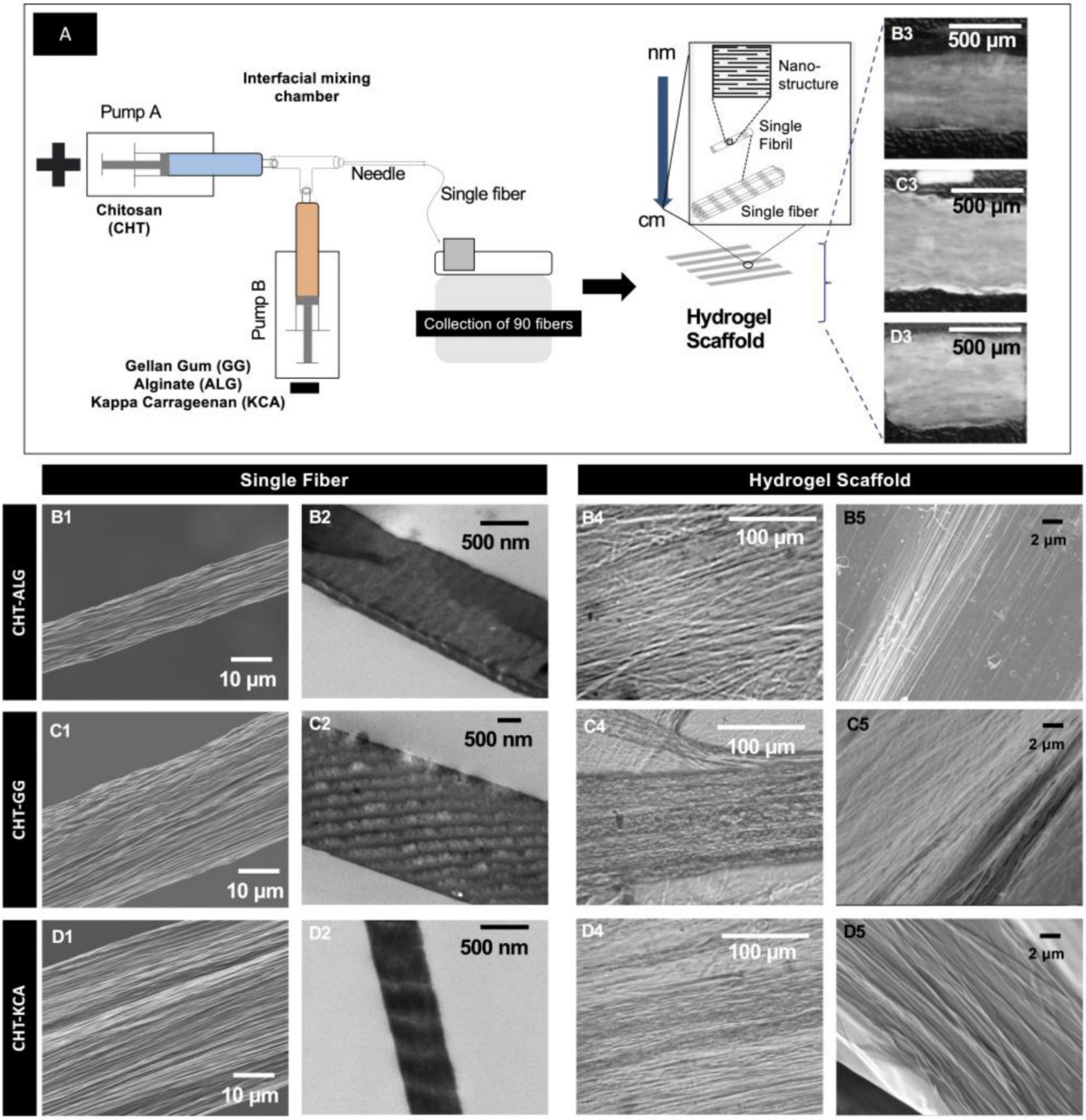

Figure 1: Fabrication and multi-scale hierarchy of three types of hydrogels

(A) Fabrication setup (left) and schematic representation of bottom-up hierarchy (right) common to the three types of hydrogels; **(B1, C1, and D1)** SEM micrographs of single fiber of CHT-ALG, CHT-GG, and CHT-KCA, respectively. **(A3, B3, and C3)** TEM micrograph showing dark and light regions with periodically varying electron density at nanoscale for single fiber of CHT-ALG, CHT-GG, and CHT-KCA, respectively. **(B3, C3, and D3)** Photographic images of CHT-ALG, CHT-GG, and CHT-KCA hydrogels, respectively; **(B4, C4, and D4)** Light microscopy images of CHT-ALG, CHT-GG, and CHT-KCA hydrogels,

respectively; **(B5, C5, and D5)** SEM micrograph showing fibrous surface of CHT-ALG, CHT-GG, and CHT-KCA hydrogels, respectively.

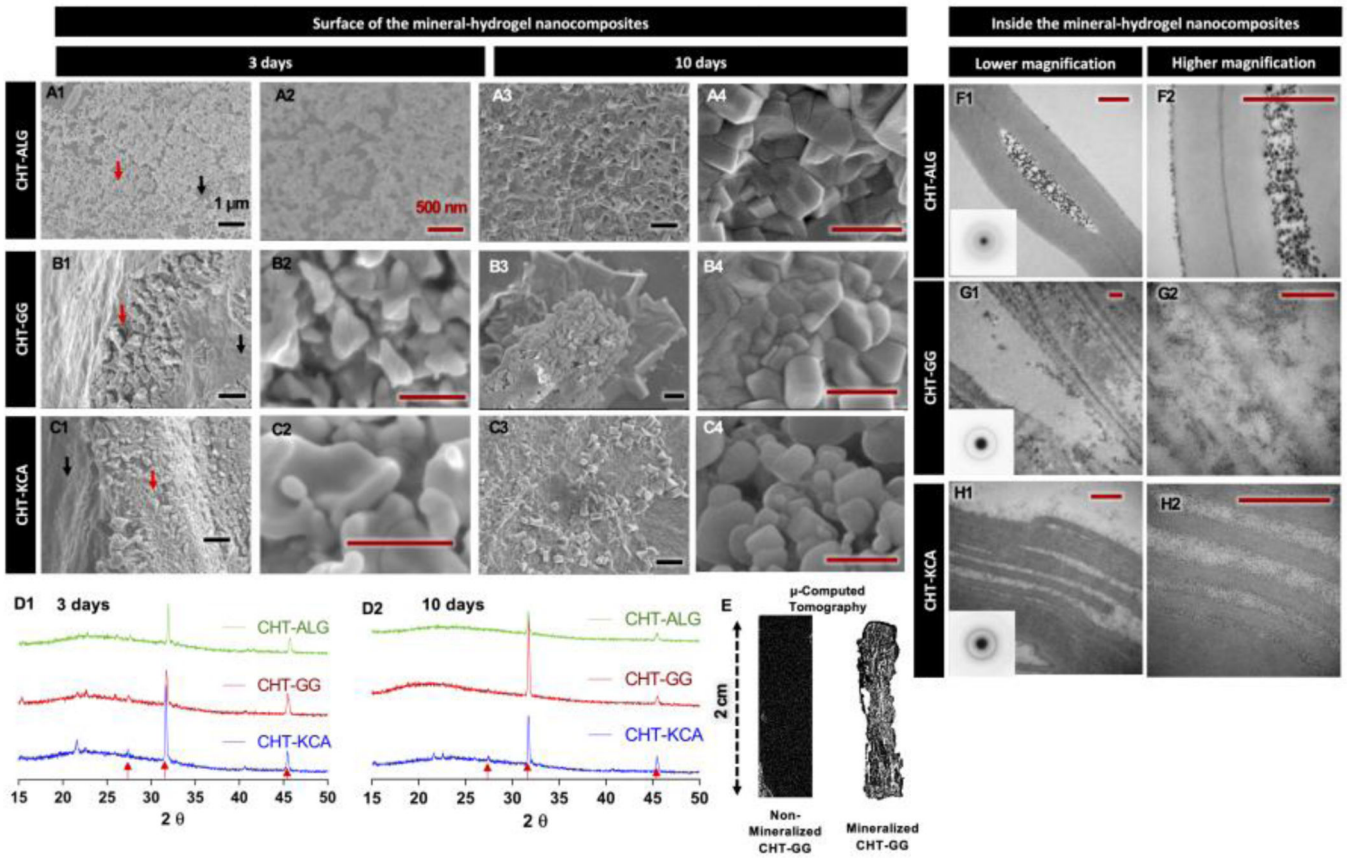

Figure 2: *In vitro* mineralization and mineral characterization

(A1-A2, B1-B2 and C1-C2) SEM micrographs of the deposited minerals (red arrow) and hydrogel area without minerals (black arrow) for three-day mineralized CHT-ALG, CHT-GG, and CHT-KCA mineral-hydrogel nanocomposites, respectively; (**A3-A4, B3-B4 and C3-C4)** SEM micrographs for ten-day mineralized CHT-ALG, CHT-GG, and CHT-KCA mineral-hydrogel nanocomposites, respectively; (**F1-F2, G1-G2, and H1-H2)** TEM images of transverse sections of three-day mineralized CHT-ALG, CHT-GG, and CHT-KCA mineral-hydrogel nanocomposites, respectively; Inset images in **F1, G1, and H1** show selected area electron diffraction patterns of the corresponding mineral-hydrogel nanocomposites type; (**D1 and D2)** XRD spectra of three-day mineralized and ten-day mineralized mineral-hydrogel nanocomposites, respectively. Red arrows indicate matching peaks with carbonated apatite; (**E)** A representative three-dimensional micro-CT image of 2 cm x 0.5 cm non-mineralized CHT-GG (left) and ten-day mineralized CHT-GG mineral-hydrogel nanocomposite. Black scale bars indicate 1 μm and red scale bars indicate 500 nm.

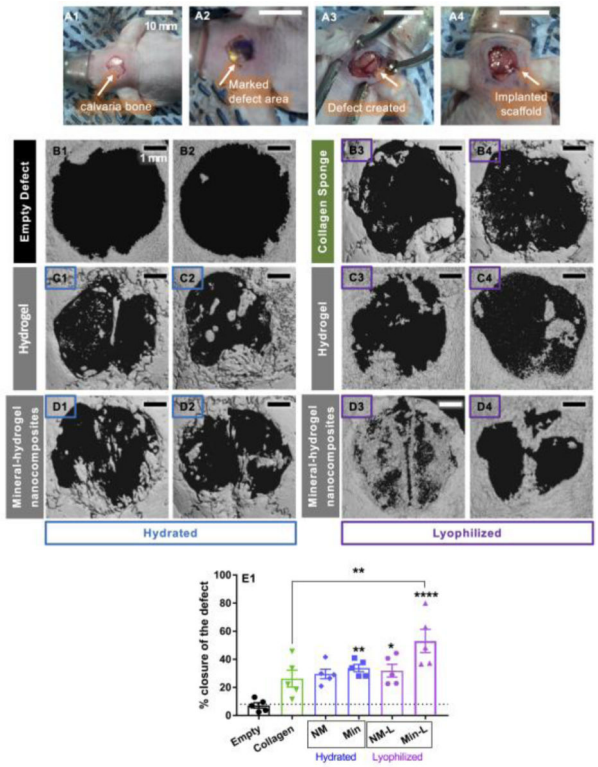

Figure 3: Closure of mouse critical sized defect 12-weeks after implantation of mineral-hydrogel nanocomposites

(A1) Calvaria bone in the skull, **(A2)** marked 5mm diameter area for creating the defect, **(A3)** calvaria bone defect exposing the brain underneath, and **(A4)** implanted hydrogel; Scale bar in A1-A4 indicate 10 mm; **(B1-B2)** Representative 3D reconstructed μCT images for empty control group (no material implanted in the calvaria defect); **(C1-C2 and D1-D2)** μCT images for CHT-KCA hydrogels (non-mineralized) and CHT-KCA mineral-hydrogel nanocomposites, respectively, in hydrated form; **(B3-B4)** μCT images for lyophilized collagen sponge, **(C3-C4 and D3-D4)** μCT images for CHT-KCA hydrogels (non-mineralized) and CHT-KCA mineral-hydrogel nanocomposites, respectively, in lyophilized form; Scale bar in B1-D4 indicate 1 mm; **(E)** a comparison of percent closure of the critical sized defect by regenerated bone quantified using FIJI * indicates statistical significance ($p<0.05$) compared to empty defect with one-way ANOVA analysis and Tu ey's post-hoc test, ** indicates $p<0.005$, **** indicates $p<0.00005$; error bars: standard error of mean; n=5. Abbreviations: NM-non-mineralized hydrogels, Min-mineral-hydrogel nanocomposite, NM-L- lyophilized non-mineralized hydrogels, Min-L- Lyophilized mineral-hydrogel nanocomposites.

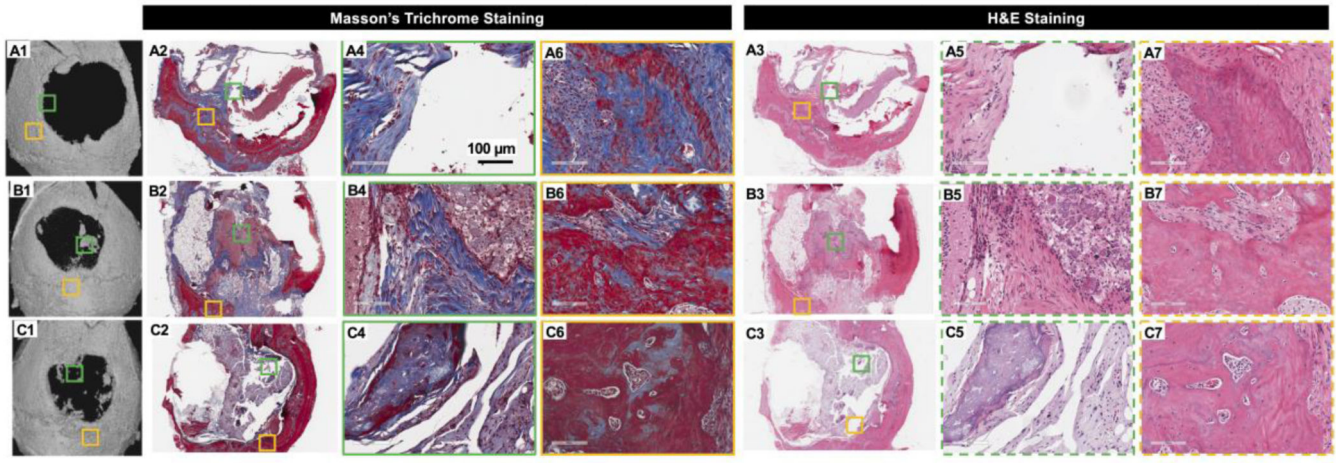

Table 1

Qualitative	New Bone Region	Native Old Bone Region
Empty	No bone growth, mostly brain tissue from underneath.	Fibrosis, hemosiderin laden macrophages, fibroblasts proliferation.
Hydrogel	Fibrosis, focal hemosiderin, focal immature bone, disorganized bone present, histiocytes, occasional lymphocytes.	Fibrosis, fibroblastic proliferation, numerous histiocytes, lining of immature bone at defect edge.
Mineral-hydrogel nanocomposites	Fibrosis, small amount of immature bone, some neutrophils, histiocytes, granulation tissue.	Small area of fibroblastic proliferation, osteoblastic rimming.

Table 2

Quantitative	Average H-score
Empty	0
Hydrogel	1
Mineral-hydrogel nanocomposites	2

Figure 4: Histological evaluation of mouse critical sized defect area 12-week after implantation of mineral-hydrogel nanocomposites

(A1, B1, and C1) μCT images of empty defect control, lyophilized CHT-KCA hydrogels, and lyophilized CHT-KCA mineral-hydrogel nanocomposites implanted mice used for histology sectioning, respectively. (**A2, B2, and C2**) Masson's Trichro e stained stitched images of longitudinal section of empty defect control, lyophilized CHT-KCA hydrogels, and lyophilized CHT-KCA mineral-hydrogel nanocomposites implanted mice, respectively; (**A3, B3, C3**) Similar H&E stained stitched image of longitudinal section of empty defect control, lyophilized CHT-KCA hydrogels, and lyophilized CHT-KCA mineral-hydrogel nanocomposites, respectively; **(A4-A5, B4-B5, C4-C5)** Magnified images from new bone region (NB) are indicated in green boxes for control, hydrogels, and mineral-hydrogel nanocomposites, respectively. **(A6-B7, C6-C7, D6-D7)** Similar images from the native old bone region (OB) are shown in yellow boxes. Solid lined boxes are used to indicate Masson's Trichro e stained i ages and dotted lined boxes are used for H&E stained images. (Table 1) Qualitative evaluation of H&E and Masson's Trichro e stained longitudinal sections of mice calvaria from two different regions (Green-NB and Yellow-OB). (Table 2) Healing score (H-score) of the same sections from NB area; Score range: 0–4; NB- new bone, OB- old native bone.